AIR FAST-COOLING TECHNOLOGY FOR 1000 MW NUCLEAR STEAM TURBINES AND ITS APPLICATION

Ming Li [1],Chunbo Li [3],Pengfei Han [1],[2], Youjun Zhang [2], Yong Yu [4], Lei Yu [4], Yingwei Liu [1], Peidong Liu[1], Zhanhui Liu[1], Xin Liu[1], Danmei Xie5, Wei Jiang [5,6*]

[1] Rundian Energy Science and Technology Co., Ltd., Zhengzhou 450018, China;

[2] China Resources Power Technology Research Institute Co., Ltd., Dongguan 523808, China;

[3] School of Power and Mechanical Engineering, Wuhan University, Wuhan 430072, China;

[4] Jiangsu Zhenjiang Generator Co.,Ltd, Zhenjiang 212000, China;

[5] Hubei Key Laboratory of Fluid Machinery and Power Engineering Equipment Technology, Wuhan University, Wuhan 430072, China

[6]Suzhou Institute of Wuhan University, Suzhou 215123, Jiangsu, China

[*] Corresponding author; E-mail: jiangwei@whu.edu.cn

The large-scale integration of renewable energy requires increased flexibility from nuclear power units in modern power systems. Steam turbines in nuclear units have low natural cooling efficiency and slow cooling rates due to their large size and intricate structure. This study investigates the application of air fast-cooling technology to enhance the shutdown speed and flexibility of a 1000 MW nuclear steam turbine, marking its first application to Hua-long Pressurized Reactor (HPR1000). The finite element method was utilized to simulate the evolution of temperature and stress fields during the air fast-cooling process. The results demonstrate that the proposed air fast-cooling scheme effectively reduces rotor temperatures. Specifically, a 40 hrs cooling period decreases temperatures across rotor surfaces to below 100°C, thereby confirming its high cooling efficiency. Moreover, the maximum thermal stress during air fast-cooling is 85.2 MPa, significantly below the material's fatigue stress limit, validating the safety of the scheme. This technology has been implemented in the fast cooling of the HPR1000, with measured cooling times showing high consistency with simulation results, confirming its safety and reliability.

Key words*: Nuclear power, Steam turbine, Air fast-cooling, Thermal stress, Flexibility*

1. Introduction

Nuclear power units, characterized by substantial capacity, zero emissions, and minimal susceptibility to natural factors, constitute a crucial component of various carbon neutrality solutions [1-4]. To enhance the efficiency of nuclear power units and reduce nuclear power costs, nuclear steam

turbines [5] are being developed to achieve higher power output[6, 7]. Nevertheless, the integration of large-scale intermittent power sources into the grid [8-10] and the residential heating demand pressures arising from the decreased reliance on coal-fired power [11] will inevitably impose additional demands on nuclear power units[12]. Therefore, the development of large-capacity nuclear power units with fast start-stop capabilities is a critical requirement for advancing nuclear steam turbines[13].

Modern nuclear steam turbines, often designed as half-speed machines with relatively low inlet steam parameters and steam density, exhibit significantly larger volumetric flow rates for equivalent power outputs compared to conventional coal-fired units[14-16]. This requires more voluminous cylinder structure and results in substantially increased thermal inertia after shutdown, prolonging natural cooling times. Especially, the widespread use of heat insulators on high-pressure (HP) cylinder further exacerbates this issue. Taking the HPR1000 unit as an example, the surface temperature of HP rotor frequently exceeds 200°C after a normal shutdown. It requires approximately 8 to 9 days for the HP rotor wall temperature decrease to 100℃, thereby allowing for the commencement of maintenance activities[17]. This process not only consumes valuable maintenance time but also delays the unit regeneration time, thereby reducing its availability and response capability to power demand. Under emergency shutdown, the cooling period may extend to 9-10 days due to the rotor and inner wall temperatures of the HP cylinder are significantly elevated. Operational experience and relevant standards from nuclear power industry stipulate that units undergo scheduled shutdown maintenance every eighteen months. During this process, the conflict between the cooling rate of the rotor metal temperature and the maintenance schedule becomes particularly acute[18]. The excessively long natural cooling times of large capacity steam turbine units not only limit unit availability but also impair their market competitiveness[19]. Therefore, the exploration and application of fast cooling technologies to shorten unit cooling time are essential for enhancing the economic performance and operational adaptability of nuclear power units[20].

Current fast cooling methods for nuclear steam turbines include steam cooling, vacuum cooling [21], and compressed air cooling[22-24], etc. Steam cooling utilizes deeply throttled low-temperature and low-pressure steam or cross-unit and auxiliary steam sources, to cool nuclear power units. This method imposes significant operational complexity, requiring strict adherence to prescribed down gradient for steam temperature and pressure. Vacuum cooling method involves drawing ambient cold air into the turbine via vacuum pumps. Its advantage lies in leveraging existing equipment for easier implementation. However, vacuum cooling suffers from slow cooling rates at lower temperatures and issues related to boiling in shaft seals.

Compressed air cooling method employs air drawn from a compressed air header. The air is purified, potentially heated, and then introduced into the steam turbine for fast-cooling. This method allows adjustable control over the cooling rate, offering strong controllability. Furthermore, due to air's low specific heat and relatively lower heat transfer coefficient compared to steam, the absence of phase-change eliminates associated risks. Consequently, compressed air cooling offers high safety, controlled cool-down characteristics, and strong feasibility.

To verify the efficacy and safety of the air fast-cooling scheme for nuclear steam turbines, this study establishes a thermo-mechanical coupling model[25] based on the complete geometry of the steam turbine cylinder and rotor. A specialized finite element model and computational methodology suitable for simulating the air fast-cooling process in nuclear steam turbines are developed[26]. The transient temperature and stress field of the steam turbine cylinder and rotor during the air fast-cooling process

are obtained. The effectiveness of the air fast-cooling scheme for steam turbines is being verified based on the transient temperature and stress field, and the safety analysis and condition assessment of the steam turbine rotor have been carried out. Results show that air fast-cooling can significantly shorten shutdown times without compromising unit lifespan, thereby reducing maintenance time and enhancing the economic efficiency and operational flexibility of the unit.

2. Numerical Method

2.1. Geometric Modeling

To accurately analyze temperature and stress fields in the steam turbine rotor under various operating conditions while minimizing boundary-induced artifacts, the geometric modeling of the steam turbine rotor[27] necessitates rational simplification. The following justified assumptions are adopted to ensure simulation fidelity:

(1) The rotor and cylinder of the steam turbine are approximately axisymmetric models. A two-dimensional (2D) cross-section domain is adopted for simulation.

(2) Adiabatic boundary conditions are applied to: the rotor's central axis of symmetry, both axial end-faces.

Consequently, ignoring some small grooves and corners on the rotor surface, the 2D geometric model of the HP rotor and cylinder of the steam turbine is shown in Fig. 1. Supporting bearings are fixed at both the left and right ends of the model, and a thrust bearing is also installed at the right end to prevent axial displacement of the rotor.

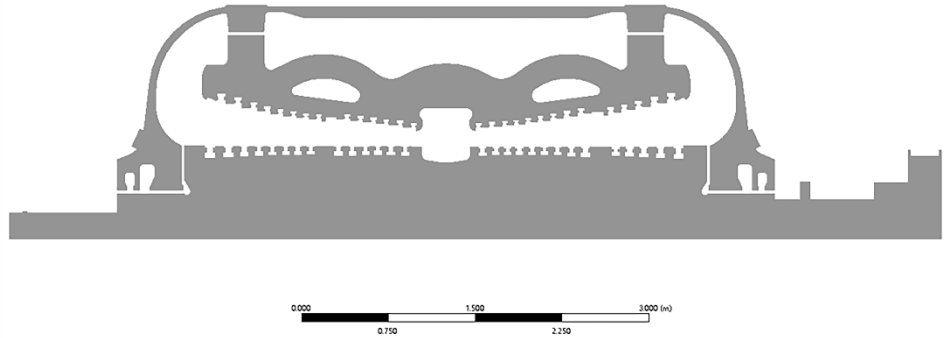

Fig. 1 Axisymmetric 2D geometric modeling of rotor and cylinder.

2.2. Meshing of Rotor and Cylinder

After accurately setting the cylinder-rotor model and the corresponding ANSYS coordinate system, the mesh of the cylinder-rotor model is automatically generated in the ANSYS Meshing platform. The unstructured meshing method is adopted[28]. On the basis of unstructured meshing, local mesh refinement is performed on the key parts of the HP rotor. The maximum mesh size is set to 20 mm. Finally, the number of mesh nodes is determined to be 32450, and the resulting meshing is shown in Fig. 2.

A mesh independence study was conducted using the steady-state value of the maximum centrifugal stress as the reference. As shown in Table 1, the maximum stress value stabilized when the number of mesh nodes exceeded 32,450, with a relative variation of only 0.42%. Considering that an excessive number of mesh elements significantly increases computational cost, a mesh size of 32,450 nodes was selected for subsequent calculations to balance computational efficiency and accuracy.

Table 1
Mesh independence verification results.

	Number of meshs	Maximum stress value/Mpa	Errors/%
1	22848	86.30	0.61
2	32450	85.78	-
3	48988	85.42	0.42

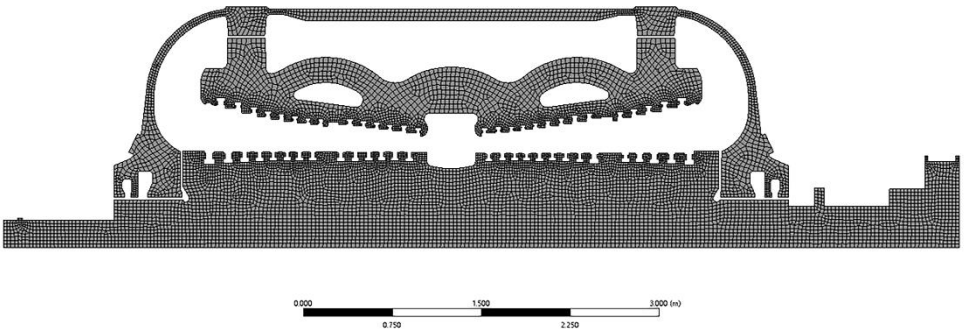

Fig. 2 Refined cylinder-rotor mesh.

2.3. Governing Equations

In finite element analysis, a heat transfer process is considered steady-state if the temperature field remains constant over time. Finite element analysis can determine parameters such as the steady-state temperature field, thermal gradients, and heat flux density. In contrast, transient thermal analysis calculates the time-dependent temperature distribution of a model. In coupled analysis, the transient temperature field is computed first, and the results are subsequently applied as thermal load boundary conditions for the stress analysis. A significant difference between the two methods lies in the heat storage effects, while negligible in steady-state analysis, these effects must be taken into account in transient analysis. Furthermore, material properties including density, thermal conductivity, and specific heat capacity must be incorporated into the calculation model.

The governing equation for thermal equilibrium in transient thermal analysis can be expressed as follows:

$$\frac{\partial}{\partial x}(k_{xx}\frac{\partial T}{\partial x})+\frac{\partial}{\partial y}(k_{yy}\frac{\partial T}{\partial y})+\frac{\partial}{\partial z}(k_{zz}\frac{\partial T}{\partial z})+q_v=\rho c_p\frac{\partial T}{\partial t} \tag{1}$$

Where q_v is the volumetric heat generation rate, and k_{xx}, k_{yy}, and k_{zz} are the thermal conductivities, ρ is the mass density, c_p is the specific heat capacity, respectively.

The correct selection of boundary conditions is essential to ensure calculation accuracy. In finite element thermal analysis, boundary conditions are generally classified into three types: temperature boundary conditions, heat flux boundary conditions, and convection heat transfer boundary conditions. The corresponding expressions are expressed as follows:

$$\begin{cases} T_w=T(x,y,x,t) \\ -\lambda(\frac{\partial T}{\partial n})_w=q(x,y,x,t) \\ -\lambda(\frac{\partial T}{\partial n})_w=h(T_w-T_f) \end{cases} \tag{2}$$

Where $T(x, y, z, t)$ is the temperature boundary function, and $q(x, y, z, t)$ is the heat flux boundary function, n is the surface normal direction, h is the convective heat transfer coefficient of the boundary wall, T_w and T_f are the wall temperature and the near-wall fluid temperature, respectively.

In this study, the nodal displacement method is adopted to calculate the stress and strain fields. In this approach, nodal displacements are treated as the fundamental unknowns of the element. Based on the principle of minimum potential energy, the finite element formulation is established. The element nodal displacement matrix is expressed as follows:

$$\{\delta\}^e = [\delta_i^y \quad \delta_j^y \quad \delta_m^y] = [u_i \quad w_i \quad u_j \quad w_j \quad u_m \quad w_m]^T \tag{3}$$

The nodal displacement matrix is expressed as follows:

$$f = \begin{Bmatrix} u \\ w \end{Bmatrix} = [N]\{\delta\}^e \tag{4}$$

Where [N] is the finite element displacement shape function. By substituting [N] into the geometric equations of the computational model, the displacement distribution of the element nodes can be determined, yielding the strain matrix:

$$\{\varepsilon\} = \{\varepsilon_r \quad \varepsilon_\varphi \quad \varepsilon_z \quad \gamma_{rz}\} = \left\{\frac{\partial u}{\partial r} \quad \frac{u}{r} \quad \frac{\partial w}{\partial z} \quad \frac{\partial u}{\partial z} + \frac{\partial w}{\partial r}\right\} \tag{5}$$

Where γ_{rz} is the shear strain column vector matrix. Based on Hooke's Law, the finite element formulation for the stress-strain relationship is obtained as follows:

$$\{R\} = [K]\{\delta\} \tag{6}$$

Where $\{R\} = \sum\{R\}^e$ is the nodal load column vector matrix, $\{K\} = \sum\{K\}^e$ is the global stiffness matrix, and $\{\delta\} = \sum\{\delta\}^e$ is the nodal displacement column vector matrix.

The Von Mises Yield Criterion was adopted to calculate the Von Mises stress and the formula for determining this equivalent stress is expressed as follows:

$$\sigma_{eq} = \sqrt{\frac{1}{2}[(\sigma_r - \sigma_\theta)^2 + (\sigma_\theta - \sigma_z)^2 + (\sigma_z - \sigma_r)^2 + 6\tau_{r\theta}^2 + 6\tau_{\theta z}^2 + 6\tau_{zr}^2]} \tag{7}$$

Where σ_{eq} is the equivalent stress. σ_r, σ_θ, and σ_z are the radial, tangential, and axial stresses, respectively. $\tau_{r\theta}$, $\tau_{\theta z}$, and τ_{zr} are the shear stress components.

2.4. Boundary Conditions of Rotor and Cylinder

For nuclear steam turbines, during the fast-cooling process, the HP rotor bears mainly centrifugal and thermal load. Therefore, the boundary conditions are divided into mechanical boundary conditions and thermal boundary conditions. Regarding the mechanical boundary conditions, the centrifugal force can be directly characterized by the rotational speed. For the supporting and thrust bearing at both ends of the rotor, displacement constraints in different directions need to be applied. Since the rotor is an axisymmetric model and its 2D model is used for simulation calculation, a radial constraint needs to be applied on the rotor centerline.

The rotor surface includes the smooth shaft, both sides of the wheel disc, the wheel rim, etc. The left and right end faces and the center of the rotor are set as heat insulation. The bearing positions at both ends are treated with the Dirichlet boundary condition (set to 55°C) because the oil return temperature is constant. The heat transfer on the cylinder and rotor surfaces belongs to the Robin boundary condition with known heat transfer coefficient and air temperature. The detailed boundary conditions are shown in Fig. 3.

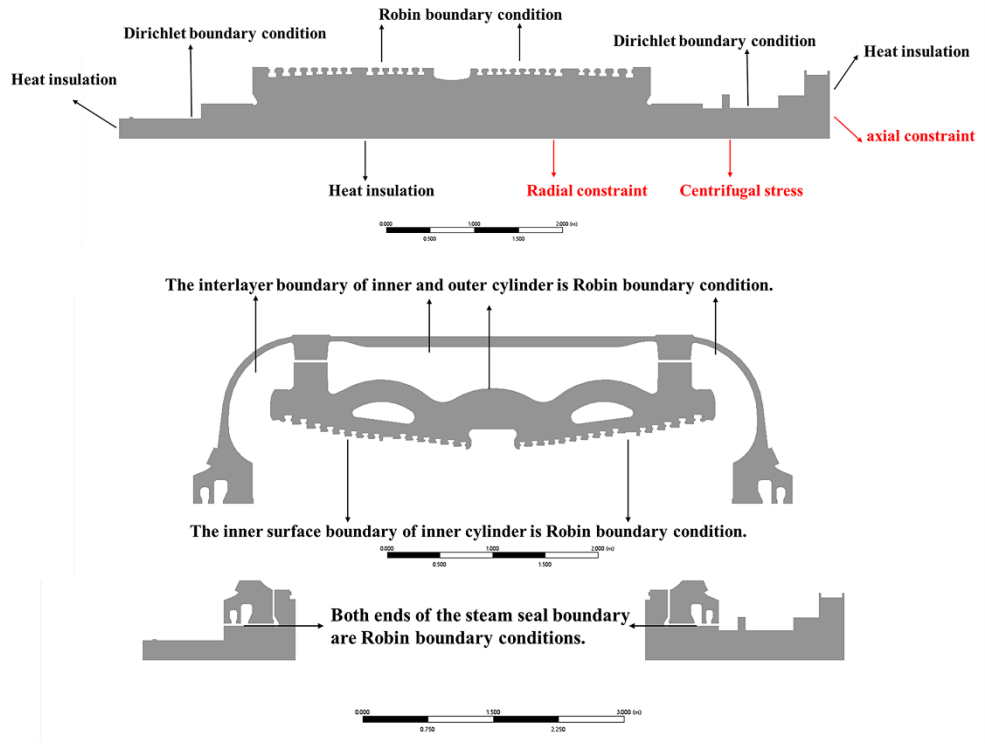

Fig. 3 Rotor and cylinder boundary conditions.

In the case of forced air cooling, the cooling air enters the cylinder, cools through the flow gap between the rotor and the inner cylinder, and then is discharged through the exhaust port. The heat transfer process between the metal surface of the rotor and the air is quite complex. This study adopts the empirical formula commonly used in the power industry for calculation. First, it is necessary to determine the dimensionless flow measurement value G_0 of the cooling air:

$$G_0 = \frac{G}{\rho \cdot n \cdot D^3} \tag{8}$$

Where G and ρ are the mass flow and density of air, D and n are the maximum diameter and rotational speed of the wheel disc, respectively.

In our work, the measured flow is initially set to 2 kg/s. Through calculation, it is found that $G_0 > 0.0004$, so the influence of limited space can be ignored. The criterion formula for cooling when the cooling air flows over the rotor side in a large space can be used:

$$N_u = \frac{hr}{\lambda} = 0.45 \cdot \beta \cdot Re^{0.8} \tag{9}$$

$$h = 0.45 \cdot \frac{\lambda \cdot \beta}{r} \cdot Re^{0.8} \tag{10}$$

$$\beta = 0.1313 + (1+\varepsilon^2)^{0.3} \cdot (0.08547 \cdot \frac{v_a}{v} + 0.3131 \cdot \varepsilon)^{0.2} \tag{11}$$

$$\varepsilon = (0.0262 + 0.4399 \cdot (\frac{v_a}{v})^2)^{0.5} - 0.009362 \cdot \frac{v_a}{v} \tag{12}$$

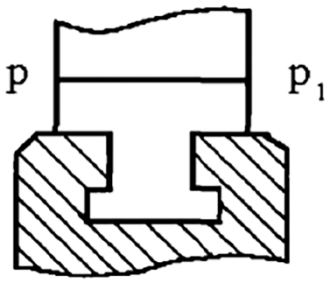

Fig. 4 Simplified structure of the wheel groove of the HP cylinder rotor.

In the study of straight fin problems, it is assumed that the convection coefficient is constant along the blade height and does not change with height. Moreover, the local heat dissipation problem in the blade tip area is not considered separately but is incorporated into the heat transfer coefficient of the blade body. The total heat transfer area of the finned surface (A) = total surface area of the fins (A_f) + surface area outside the fin surface (A_b). The heat transferred through A_b:

$$Q_b = h \cdot (\theta_0 - t) \cdot A_b \tag{13}$$

the heat transferred through A_f:

$$Q_f = \phi \cdot h \cdot (\theta_0 - t) \cdot A_f \tag{14}$$

Where h is the convection coefficient, θ_0 is the temperature at the root of the fin, t is the temperature of the surrounding fluid, and φ is the fin efficiency.

$$Q = Q_b + Q_f = h \cdot (\theta_0 - t) \cdot [A - A_f \cdot (1 - \varphi)] = h \cdot p \cdot (\theta_0 - t) \cdot A \tag{15}$$

$$h_p = \frac{h \cdot (A_b + \varphi A_f)}{A_p} \tag{16}$$

Where h_p is the equivalent heat transfer coefficient of pp1, A_p is the annular area of pp1($A_p = 2\pi \cdot r_p \cdot l$), Ab is the surface area outside the fin surface ($A_b = A_p - A_p \cdot l \cdot n$), A_f is the total surface area of the fins (Af = L·h), r_p is the impeller radius of pp1, l is the axial chord length, Apl is the cross-sectional area of the blade (approximately $A_p/2$), n is the number of blades, L is the perimeter of the blade cross section, h is the blade height, respectively.

3. Air Fast-Cooling Scheme

The air fast-cooling scheme adopts compressed air entering the HP cylinder in a downstream manner for forced cooling. First, the cooling air enters the main steam pipe through the fast-cooling interface on the control valve, then enters the interior of the HP cylinder from the upper and lower inlets in the middle of the HP cylinder through the main steam pipe, and is discharged from the steam exhaust port after completing the cooling process. It is necessary to ensure that the rotor stress is less than 300 MPa during the entire fast-cooling process. The minimum temperature of the compressed air is approximately 30 ℃, but considering the heating capacity of the fast-cooling device, the maximum temperature is set to 150 ℃. Meanwhile, considering the heating from the compressor, the minimum temperature is set to 40 ℃ or 45 ℃. Approximately taking the average of the maximum and minimum temperatures, the intermediate temperature is set to 100 ℃. In order to compare the influence of compressed air temperature on fast-cooling efficiency, three different schemes are adopted, in which compressed air with different temperatures is introduced in different time stages. When the unit is operating under full-power steady-state conditions, if an emergency occurs requiring an emergency

shutdown, air fast-cooling is immediately activated. To simulate this working condition, the following three schemes are designed.

Fast-Cooling Scheme 1: First, cooling air at 150 ℃ is introduced for 1 hr, then cooling air at 100 ℃ for 1 hr, and finally cooling air at 40 ℃ for 38 hrs, with a total time of 40 hrs.

Fast-Cooling Scheme 2: First, cooling air at 150 ℃ is introduced for 1 hr, then cooling air at 100 ℃ for 2 hrs, and finally cooling air at 40 ℃ for 37 hrs, with a total time of 40 hrs.

Fast-Cooling Scheme 3: First, cooling air at 150 ℃ is introduced for 1 hr, then cooling air at 45 ℃ for 39 hrs, with a total time of 40 hrs.

The effectiveness of the air fast-cooling scheme lies in optimizing the way of introducing cooling air and evaluating the cooling effect across varying temperatures and durations of cooling air, with the aim of determining the optimal scheme. Fig.5 shows the changes of initial air temperature, air flow rate and rotational speed with time for the three schemes during the fast-cooling process.

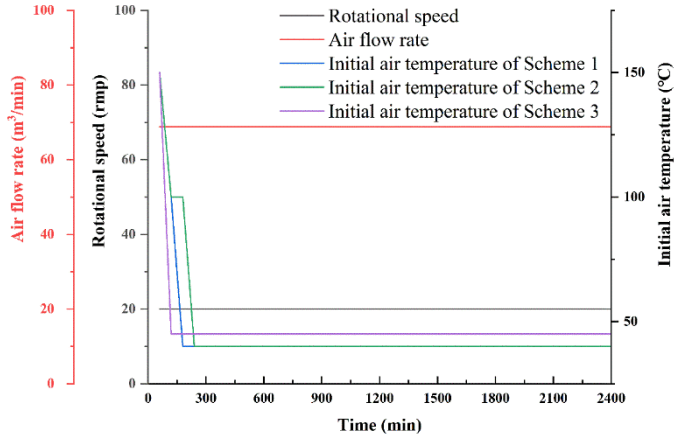

Fig. 5 Parameter variation curves under different fast-cooling schemes.

4. Results and Discussion

4.1. Temperature Field of Rotor and Cylinder

Prior to shutdown, the turbine rotor operates under sustained high-speed rotational conditions with nominal steam flow traversing its surface. The different steam parameters and flow states at different positions lead to different heat transfer conditions. Fig. 6 shows the initial steady-state temperature field of the rotor at shutdown. It can be found that the axial temperature difference of the rotor is large, while the radial temperature difference is small. The peak temperature of 274.98°C occurs at the first-stage HP rotor.

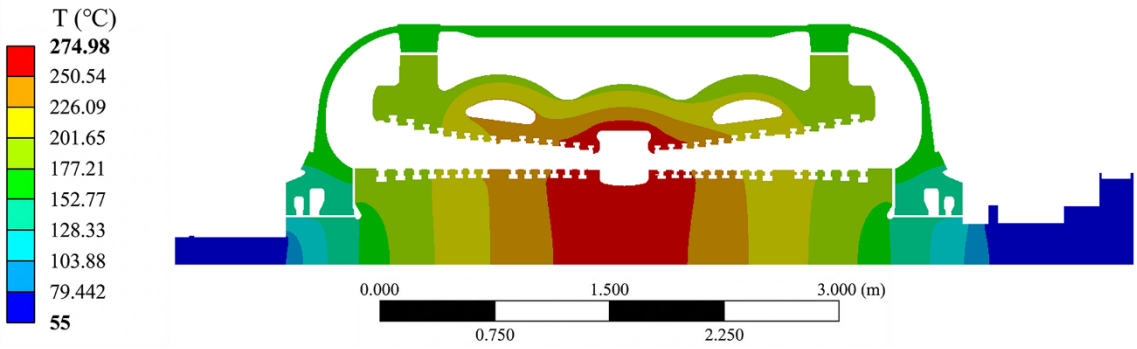

Fig. 6 Initial steady-state temperature field of nuclear power turbine high-pressure cylinder.

For the numerical simulation of the transient temperature fields of the rotor and cylinder during the air fast-cooling process, based on the boundary conditions and the calculated operating data, the heat transfer coefficients and temperatures of different parts are calculated. Meanwhile, the steady-state temperature field of the rotor is applied as the initial condition for transient analysis. Thus, the temporal variation in temperature at each rotor position during the shutdown process can be obtained. Fig. 7 shows the transient temperature fields at 60, 1264, 2324 mins, and at the end of the 40-hr calculation during the air fast-cooling process, respectively. It can be seen that the temperature of the rotor increases from the surface toward the center. The cooling rate at the center of the rotor is significantly lower than that at the rotor surface.

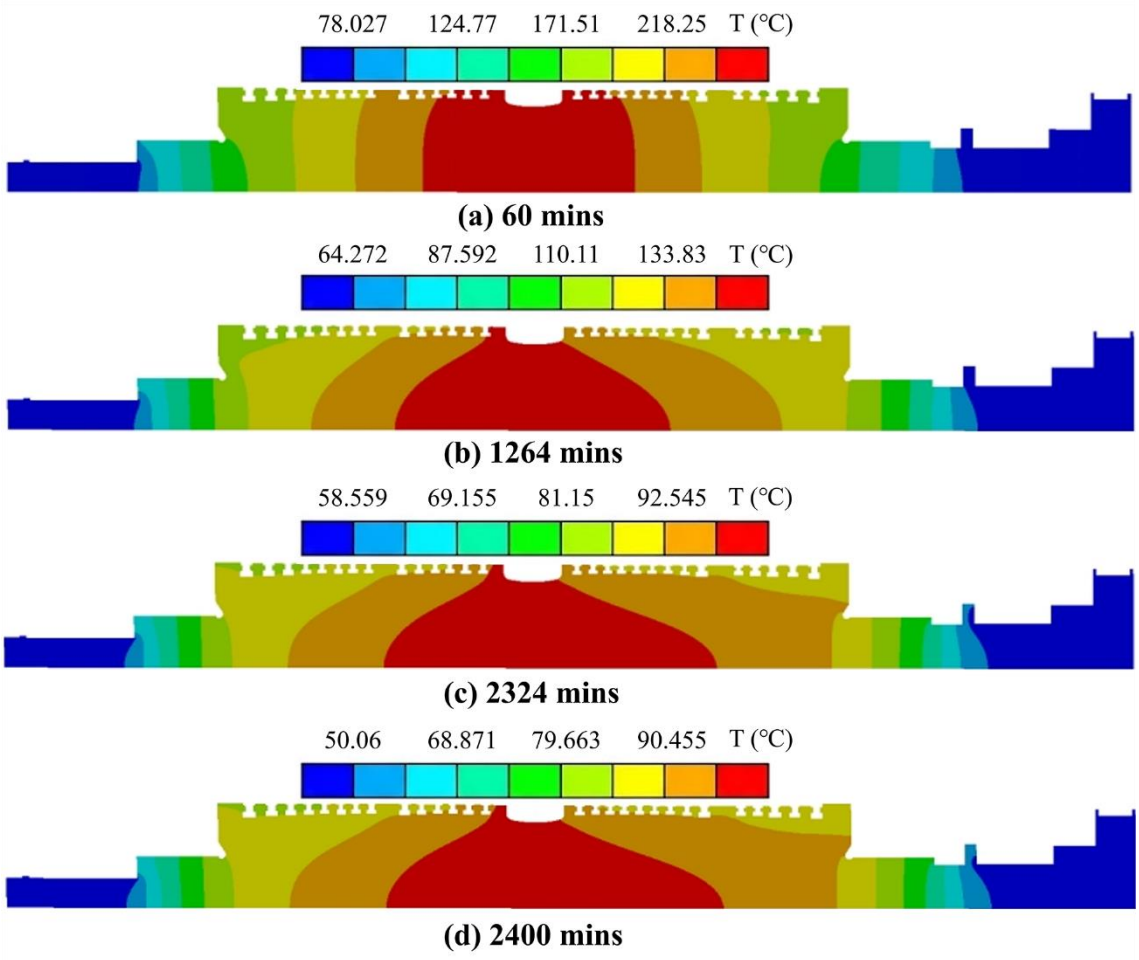

Fig. 7 Temperature field variation during steam cooling of nuclear power turbine.

Calculations performed in line with the three schemes generate the curves depicting the decline of the rotor's maximum temperature under varying compressed air temperatures, as shown in Fig. 8 (a). It can be seen that the maximum temperature of the HP cylinder rotor requires 1264, 1284, and 1277 mins to drop below 150°C, and 2324, 2354, and 2400 mins to fall below 100°C, respectively. Experimental tests revealed that the temperature dropped to 100°C after 2436 mins.

The temperature drop rates of the three schemes are showed in Fig. 8 (b). It can be seen that reducing the temperature of the incoming compressed air results in a sudden surge in the temperature drop rate followed by a gradual decay. Outside of this phase, the temperature drops rate remains below 10°C/h. Among these, Scheme 1 and Scheme 2 employ a three-stage cooling method, and the average

temperature drop rate of the rotor is lower than that of Scheme 3, which adopts a two-stage cooling method.

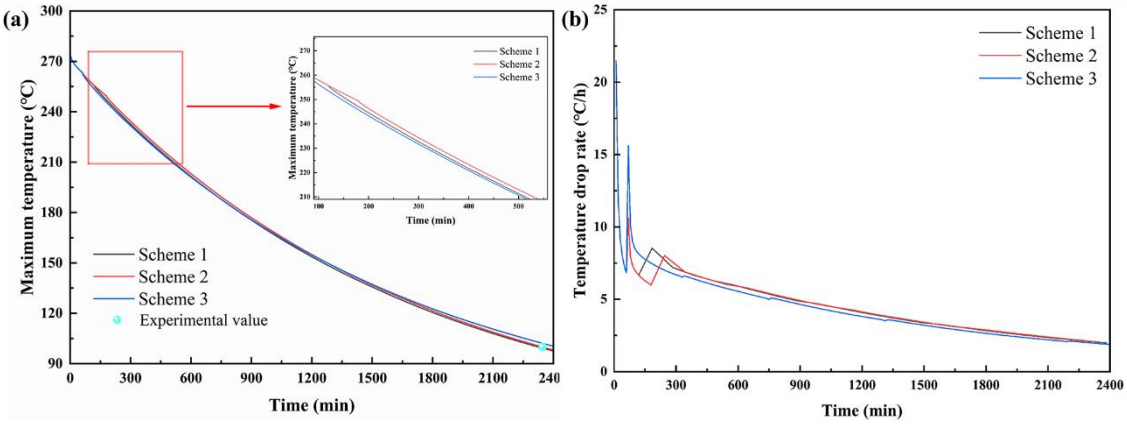

Fig. 8 (a)Temperature variation of rotor surface and center in the inlet area during air cooling. (b) Comparison of temperature drop rates under three fast-cooling schemes.

4.2. Rotor Stress Field

In Scheme 1, the stress field of the HP cylinder after 40 hrs is shown in Fig. 9. Thick-walled components are more prone to generating thermal stress during the fast-cooling process. By comparing the geometric characteristics of the rotor and analyzing the finite element calculation results, it is determined that the points with relatively high stress on the rotor are mainly concentrated at the wheel groove positions of the blade roots. To conduct a more in-depth and precise analysis of thermal stress evolution in the rotor, several key points are selected for comparative assessment, with the positions are shown in Fig. 10. These four points are located at the circular groove of the rotor shaft shoulder with maximum stress concentration, the rotor steam inlet area, the disk groove at the 6th stage of the turbine end and the disk groove at the 9th stage of the generator end.

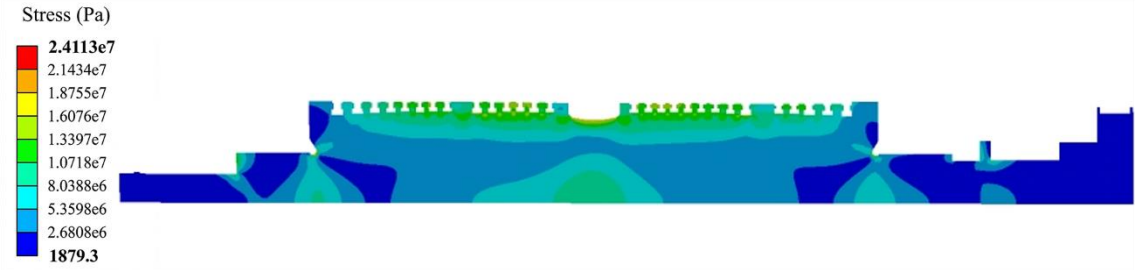

Fig. 9 Stress field after 40 hrs of fast Cooling Scheme 1.

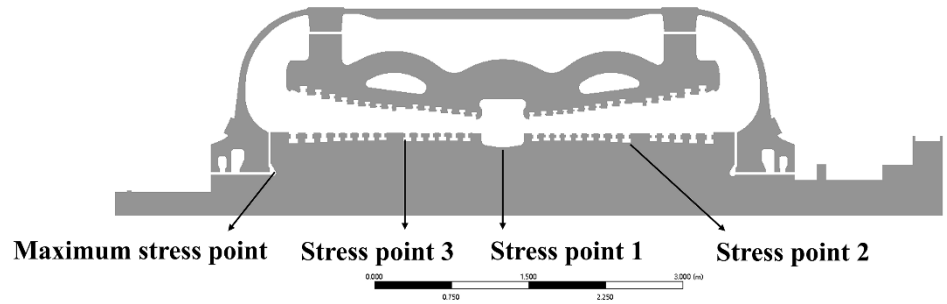

Fig. 10 Selected points for stress field analysis.

The stress variation values of the four selected points in the above figure are output and generate trend curves. The stress variation trends of the four points are shown in Fig. 11 (a). Based on the analysis of the stress peaks and variation trends of each point, it can be concluded that the maximum stress of the rotor during the fast-cooling process is approximately 85.2 MPa, and the maximum stress at the other three positions is approximately 80.1 MPa.

The comparison of maximum stress variations among the three schemes is shown in Fig. 11 (b). It can be concluded that since the initial stage is the same for all schemes, with 150℃ cooling compressed air introduced, the calculated stress variations are identical. As the fast-cooling proceeds, the rotor temperature decreases, and the maximum stress of the rotor first increases and then decreases, with similar stress variation trends observed across the three schemes. The maximum stress of the rotor occurs at the shaft shoulder circular groove, followed by the steam inlet area. Due to the forced convection effect of the cooling air at the initial fast-cooling process, the thermal stress increases significantly and quickly reaches the maximum value. With the continuous forced cooling, the rotor temperature achieves stationary equilibrium, causing the resulting thermal stress to gradually decrease and dissipate. Expectedly, the thermal stress remains within the safe range, far below the allowable value of 300 MPa that would affect the rotor's service life. Among the schemes, Scheme 1 and Scheme 2 adopt three-stage cooling, and the second stress peak of the rotor is smaller than that of Scheme 3, which uses two-stage cooling. This indicates that multi-stage cooling is beneficial for controlling the rotor's temperature drop rate and maximum stress.

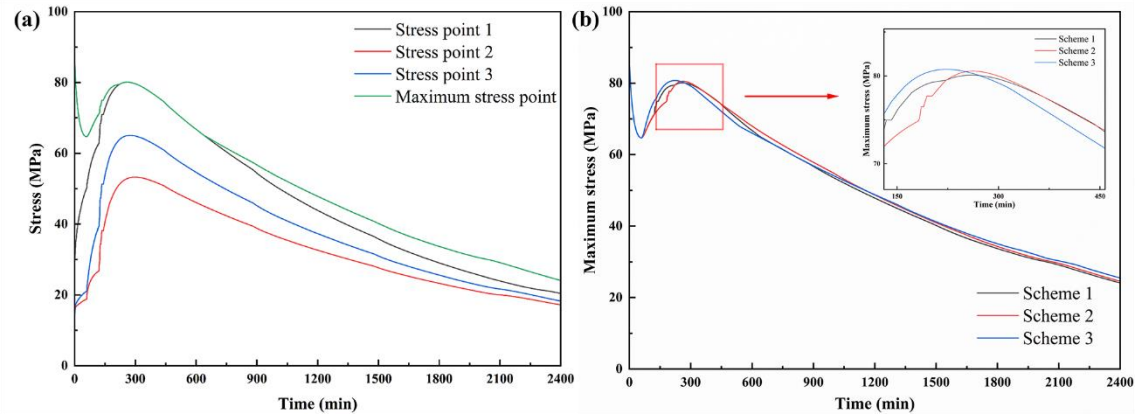

Fig. 11 (a) Stress variation trend of fast-Cooling Scheme 1. (b) Comparison of maximum stress variations among the three schemes.

Fig. 12 shows the axial deformation of the cylinder and rotor in Scheme 1, which is the fastest cooling scheme among the three fast-cooling schemes. It can be seen from the maximum deformation of the rotor and cylinder that during the air-cooling process, the axial deformation of both the rotor and the cylinder decreases, with the rotor's deformation decreasing faster and more significantly. The differential deformation analysis reveals the expansion difference between the rotor and the cylinder decreases from 2.9 mm to 1.1 mm. Therefore, there is no risk of axial impact and friction.

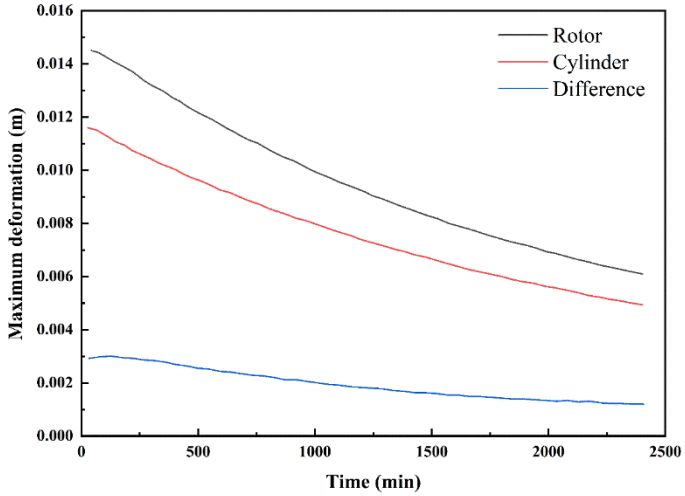

Fig. 12 Axial deformation of the cylinder and rotor in fast-Cooling Scheme 1.

5. Conclusions

In this study, the transient temperature field and stress field of the 2D axisymmetric model of the rotor and cylinder within 40 hrs of air-cooling are obtained through finite element analysis. The cooling effect and safety of the air-cooling scheme are evaluated, with detailed analysis conducted accordingly. The main conclusions are as follows:

(1) During the air fast-cooling process, the convective heat transfer coefficient on the rotor surface is small, ranging between 4~9 W/(m^2·℃), which is close to natural convective heat transfer. Therefore, the compressed air fast-cooling scheme possess inherent safety, and its cooling rate is relatively slower than that of the steam fast-cooling scheme.

(2) All three schemes can reduce the maximum temperature of the rotor surface to 100℃ within 40 hrs, indicating the effectiveness of compressed air cooling in achieving fast-cooling of the rotor and cylinder. Among them, Scheme 1 has the fastest cooling rate, which can reduce the maximum temperature of the rotor surface to 100℃ in about 38.7 hrs.

(3) The maximum temperature drop rate on the rotor surface is approximately 22℃/h, which occurs at the initial cooling phase. For most of the time, the temperature drop rate on the rotor surface does not exceed 10℃/h.

(4) During the compressed air-cooling stage, the maximum stress of the rotor is 85.2MPa, which is much lower than the allowable value of 300 MPa that would affect the rotor life. The maximum stress of the rotor occurs at the shaft shoulder circular groove, followed by the steam inlet area. Among the three schemes, Scheme 2 has the smallest mean stress.

(5) Air fast-cooling significantly reduces cooling time for nuclear steam turbines, enhancing operational flexibility while boosting economic viability through improved capacity factors. Therefore, this demonstrates strong potential for broader deployment within nuclear power systems.

Acknowledgment

This work was supported by National Natural Science Foundation of China [grant numbers 52306046] and Natural Science Foundation of Jiangsu Province [grant numbers BK20230266]. The numerical simulations in this work have been done on the supercomputing system in the Supercomputing Center of Wuhan University.

References

[1] Mallapaty, S., How China could be carbon neutral by mid-century, Nature, 586 (2020), 7830, pp. 482-483

[2] Sepulveda, N. A., et al., The Role of Firm Low-Carbon Electricity Resources in Deep Decarbonization of Power Generation, Joule, 2 (2018), 11, pp. 2403-2420

[3] Hui, L., et al., Analysis and Reflection on the Development of Power System Towards the Goal of Carbon Emission Peak and Carbon Neutrality, Proceedings of the CSEE, 41 (2021), 18, pp. 6245-6258 (in Chinese)

[4] Zarzycki, R., Panowski, M., Increase of thermal efficiency of cogeneration plant by waste heat utilisation with absorption heat pump, Thermal Science, 23 (2019), Suppl. 4, pp. 1101-1112

[5] Grkovic, V., Doder, D., Competitiveness of power systems with nuclear power plants and with high participation of intermittent renewable energy sources, Thermal Science, 26 (2022), 3 Part A, pp. 2093-2102

[6] Jinyuan, S., et al., New Progress and Development Direction of Steam Turbines in China, Journal of Chinese Society of Power Engineering, 41 (2021), 7, pp. 542-550 (in Chinese)

[7] Jaszczur, M., et al., Thermodynamic analysis of high temperature nuclear reactor coupled with advanced gas turbine combined cycle, Thermal Science, 23 (2019), Suppl. 4, pp. 1187-1197

[8] Davis, S. J., et al., Net-zero emissions energy systems, Science, 360 (2018), 6396

[9] Jenkins, J. D., et al., The benefits of nuclear flexibility in power system operations with renewable energy, Applied Energy, 222 (2018), C, pp. 872-884

[10] Yu, W., et al., A preliminary study on the coordinated development of nuclear and renewable energy power generation in China, Renewable Energy Resources, 39 (2021), 8, pp. 1069-1077 (in Chinese)

[11] Zhang, J., Path Exploration for Promoting Low-Carbon Transformation of Heating under the Background of Carbon Peaking and Carbon Neutrality, Energy of China, 43 (2021), 9, pp. 32-37 (in Chinese)

[12] Thellufsen, J. Z., et al., Cost and system effects of nuclear power in carbon-neutral energy systems, Applied Energy, 371 (2024), p. 123705

[13] Deepak Selvakumar, R., et al., Economic feasibility analysis of LHTES integration with a nuclear power plant, Applied Energy, 392 (2025), p. 126026

[14] Cao, L., et al., Analysis on flow separation characteristics of last stage blade in steam turbine under small volume flow condition, Thermal Science, 23 (2019), 5 Part B, pp. 3239-3250

[15] Yang, Y., et al., A prediction method of temperature distribution and thermal stress for the throttle turbine rotor and its application, Thermal Science, 21 (2017), suppl. 1, pp. 267-274

[16] Faizan, M., Afgan, I., Dynamic Assessment and Optimization of Thermal Energy Storage Integration with Nuclear Power Plants Using Machine Learning and Computational Fluid Dynamics, Applied Energy, 391 (2025), p. 125939

[17] Jiang, L., Exploration of Turbine No-Load Cooling Standard in Hongyanhe Nuclear Power Unit's Overhaul, Northeast Electric Power Technology, 42 (2021), 10, pp. 60-62 (in Chinese)

[18] Santini, L., et al., On the adoption of carbon dioxide thermodynamic cycles for nuclear power conversion: A case study applied to Mochovce 3 Nuclear Power Plant, Applied Energy, 181 (2016), pp. 446-463

[19] Wang, Y., et al., Power generation-cooling water Nexus: Impacts of cooling water shortage on power system operation - a simulation case study in Illinois, U.S, Applied Energy, 377 (2025), B, p. 124440
[20] Al Kindi, A. A., et al., Thermo-economic assessment of flexible nuclear power plants in future low-carbon electricity systems: Role of thermal energy storage, Energy Conversion and Management, 258 (2022), p. 115484
[21] Shi, J., et al., Application and Analysis of Rapid Cooling System for Siemens 1000MW Steam Turbine, Electric Power, 48 (2015), 11, pp. 7-12 (in Chinese)
[22] Wang, Y., Ding, X., Research and Application of Rapid Cooling Technology for a 600 MW Steam Turbine, Power Equipment, 27 (2013), 4, pp. 233-236 (in Chinese)
[23] Weinan, H., et al., Fast Cooling Scheme of 1 000 MW Nuclear Steam Turbines, Thermal Turbine, 48 (2019), 4, pp. 254-259 (in Chinese)
[24] WU, X., et al., Analysis on Rapid Cooling Technology in a 1 000 MW Steam Turbine and its Application, Electric Power, 52 (2019), 2, pp. 158-164 (in Chinese)
[25] Xianlong, L., et al., Rotor Thermostructure Coupling Analysis of Steam Turbine Start-up Process in PWR Nuclear Power Plant, Science Technology and Industry, 23 (2023), 24, pp. 232-237 (in Chinese)
[26] Hongchao, D., et al., Research of Steam Turbine Rotor Temperature and Stress Field During Cold Startup, Process Equipment & Piping, 61 (2024), 1, pp. 63-69 (in Chinese)
[27] Zhang, R., Fatigue damage analysis of steam turbine rotors based on finite element analysis, China High and New Technology (2023), 21, pp. 22-24 (in Chinese)
[28] Yulei, F., et al., Research on Grid Division in Finite Element Stress Calculation of Steam Turbine Rotor, Turbine Technology, 65 (2023), 6, pp. 406-450 (in Chinese)

Paper submitted: 25 September 2025
Paper revised: 17 December 2025
Paper accepted: 20 December 2025